Principles and Mechanisms of Strain-Dependent Thermal Conductivity of Polycrystalline Graphene with Varying Grain Size and Surface Hydrogenation

Anran Wei [a,b], Qihao Liu [a], Haimin Yao [c], Ye Li [a], Yinfeng Li [a,b,*]

[a] Department of Engineering Mechanics, School of Naval Architecture, Ocean and Civil Engineering (State Key Laboratory of Ocean Engineering), Shanghai Jiao Tong University, Shanghai 200240, China

[b] Collaborative Innovation Center for Advanced Ship and Deep-Sea Exploration, Shanghai 200240, China.

[c] Department of Mechanical Engineering, The Hong Kong Polytechnic University, Hong Kong, China

Abstract In this paper, the thermal conductivities (κ) of polycrystalline graphene (PG) with varying average grain size are investigated using Reverse Non-Equilibrium Molecular Dynamics method. Due to the presence of grain boundary (GB), the κ of PG is found to depend on the average grain size as well as in-plane strain and hydrogenation coverage. The principles and mechanisms for the change of κ with in-plane strain and surface hydrogenation are interpreted combining thermal transport theory and phonon density of states (PDOS) analysis. The thermal property of PG under tension is found to be related with the average stress in PG as a result of the suppression of Mean Free Path (MFP) and the softening of phonon modes. PG with fine grains exhibits more reduction of κ than the PG with coarse grains does under same tensile strain due to the more stress concentration at GBs. The mechanism is also revealed for the size effect on the thermal property of PG under compression. Additionally, the dependency of κ on surface hydrogenation of PG is investigated, and an unexpected two stages evolution of κ with hydrogenation coverage is interpreted preliminarily from the circumference and arrangement of functionalized domains. The negative effect of GB on the thermal conductivity is weakened significantly under full hydrogenation. Furthermore, the coupling effect between hydrogenation and strain on the κ of PG is revealed, and the thermal conductivity of PG becomes insensitive to the in-plane strain under the higher hydrogenation. These results provide new insights into the role of GB on the thermal manipulation of PG and offer theoretical basis and guideline for the design of graphene based flexible devices for thermoelectric and thermal management applications.

* Corresponding author. Tel: (86)21-34207649. E-mail address: liyinfeng@sjtu.edu.cn (Y. Li)

1. Introduction

As a 2D plate-like single layer nanomaterial gifted with exceptional properties in terms of chemical[1-2], electrical[3], mechanical[4] and optical characteristics[5], graphene has attracted a great deal of research attention over the last decades[6-7]. Graphene is not only a good conductor of electricity with zero band gap[8] and remarkable electron mobility compared to silicon[9], it has also been well known for its outstanding thermal property with a bunch of potential applications[10]. Recently, experimental investigations showed that pristine graphene possesses abnormal thermal conductivity of 2500-5000 W/mK[11-12]. A number of interesting thermal properties of graphene nanoribbons has been reported, including the anisotropy of thermal conductivity caused by the edge effect[13], thickness-dependent thermal conductivity[14], size-dependent thermal conductivity[15] and thermal rectification[16-17]. With the development of nanotechnology, a critical challenge in many nanoelectronic systems is the highly efficient heat dissipation requirement for ensuring the performance and lifetime of nanodevices, and Graphene has been acknowledged as a promising thermal material to be used in next-generation nanoelectronic devices.[18-19]

Currently, Chemical Vapor Deposition (CVD) is the most common fabrication technique for the production of large-area graphene[20-21]. However, grain boundary (GB) defects are unavoidably present in the graphene fabricated by CVD method since each grain in metallic substrate could be a nucleation site for individual grains of graphene[22-23]. Moreover, it has been confirmed that GB as a typical defective structure in polycrystalline graphene (PG) plays an important role in its mechanical[24-26], thermal[27] and electrical properties[28]. In bulk polycrystalline materials, like metals, the yielding

strength is mainly determined by the interactions between dislocations and GBs rather than by strength of the single-crystalline grains. This correlation is well established as the HallPetch relation[29-30]. In nanoarchitectures, the volume ratio of the GB regions is much more crucial due to the constituting nanoscale units, and their influence on the nanoarchitecture mechanical properties becomes highly sensitive. Therefore, understanding the role of GB is a key for fabricating high-performance nanoarchitectures[31]. Thus, for the applications of large area CVD-grown PG in thermal management, investigation into the effects of GB on its thermal properties is in great demand. Bagri *et al*. have studied the thermal conductance of ideally distributed straight GBs in PG with fixed grain size[32]. The effect of grain size on the thermal conductivity of PG with randomly distributed GBs has also been investigated[33-35].

To achieve enhanced functionalities, the thermal conductivity of graphene should also be tunable according to the requirements for the specific applications. With the advancement in the synthesis and assembly of 2D nanomaterials[36], graphene can be effectively modified via surface functionalization with other adatoms. Hydrogenation has been widely accepted as an efficient way to manipulate the properties of graphene[37-39]. And the investigations about the effect of hydrogen functionalization on thermal conductivity of pristine graphene have been reported recently[40-41], which considered that the hydrogen atoms are distributed randomly on the surface of pristine graphene. Density functional theory (DFT) calculations have shown that hydrogen adsorptions on carbon atoms at GBs are energetically more favorable than that at internal pristine grain[42]. Considering the diverse grain sizes of the PG in practical applications, the investigation

about the roles of GB on thermal conductivity of PG with surface functionalization are not only important in understanding the basic thermal characteristics of graphene, but also crucial to its application in nanoelectronic. Mu *et al*. reported the thermal conductivity of oxidized polycrystalline graphene (PG) using molecular dynamics simulation, and found that the κ of oxidized PG decreases as oxygen (O) coverage increases[43]. Here, the thermal conductivities of PGs with varying hydrogen coverages (H-coverages) are calculated and a serious of thermal characteristic of PG with surface hydrogenation is revealed. Moreover, strain effect has been reported as an efficient method to modulate the thermal conductivity of pristine graphene continuously[44], which is also avoidable in flexible graphene based devices either at microscale or nanoscale[33]. The influences of applied tensile and compressive strain on the thermal conductivity of PG and the underlying mechanisms have not been fully demonstrated yet. It has been reported that high stress concentration occurs at the GBs under applied strain affects the thermal property of PG[45]. Thus, in this paper, the thermal conductivities of PG under strains of different magnitudes and directions are investigated and interpreted systematically. The role of GB on change of κ with in-plane strain and surface functionalization are interpreted combining thermal transport theory and phonon density of states (PDOS) analysis. Our results provide useful guideline for the thermal characterization and management of PG based flexible devices.

2. Computational Method

For all the simulations in this paper, the method of Reverse Non-Equilibrium Molecular Dynamics (RNEMD)[46] is adopted for studying the thermal properties of

graphene using LAMMPS package[47]. The interaction between carbon atoms is described by the Adaptive Intermolecular Reactive Empirical Bond Order potential (AIREBO)[48], which has been widely adopted for studying the thermal and mechanical properties of carbon-based nanomaterials[49-51]. The key idea of the RNEMD method is to apply a heat flux across the system and obtain the temperature profile along the direction of heat flux to determine the temperature gradient.

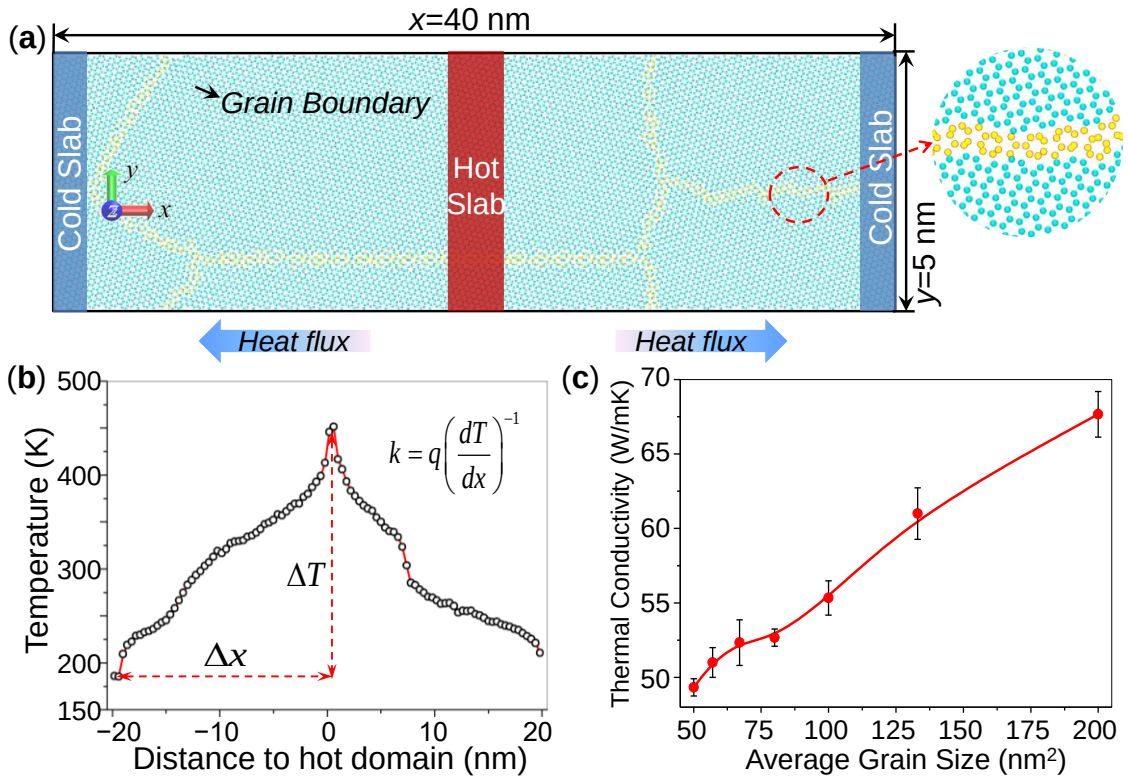

Figure 1. Reverse Non-Equilibrium Molecular Dynamics simulations for the thermal conductivity of polycrystalline graphene with an average grain size of 200 nm^2. (***a***) Atomistic structures of polycrystalline graphene under the RNEMD simulation. The cold slabs are placed at the ends of the simulation cell, while the hot slab is located in the middle. Grain boundaries composed of pentagon-heptagon defects are colored in yellow. And the carbon atoms in graphene grains are colored in cyan. (***b***) The temperature profile of polycrystalline graphene after reaching equilibrium. (***c***) The evolution of thermal conductivity with average grain size. Error bar shows the fluctuation caused by the orientation and distribution of GBs.

Figure 1a shows the illustration of the RNEMD simulation for PG. The polycrystalline structure contains randomly distributed GBs. GB triple junctions are generated using a Python code that has been successfully applied to study the toughness and strength of nanocrystalline graphene[52-53]. The GB is composed of a series of pentagon-heptagon defects as shown by the zoomed view in Figure 1a. GBs are randomly oriented for a given average grain size, and carbon atoms in the domain of GB are colored in yellow. Here, the average grain sizes are defined by dividing the simulation size by the number of grains. Periodic boundary condition is applied along both *x*-direction (parallel to the heat flux) and *y*-direction (perpendicular to the heat flux). All the PG studied in our simulations have the same length (x =40 nm) and width (y =10 nm). The thickness of PG is assumed to be 0.34 nm as suggested in previous a study[54]. All the PG in our simulations are fully relaxed at room temperature (300 K) using the Nosé−Hoover thermostat (to simulate NVT ensemble) for 10^5 time steps with τ=0.01 fs before applying a heat flux.

To obtain the temperature profile in graphene, we divide the system into many narrow slabs along *x*-direction with equal width around 0.4 nm. The temperature in each slab can be determined by[55]:

$$T_{slab} = \frac{2}{3Mk_B}\sum_j \frac{p_j^{\,2}}{2m_j}. \qquad (1)$$

where M is the number of atoms in the slab, m_j and p_j represent the mass and momentum of atom j respectively, and k_B is the Boltzmann constant. Then the temperature profile along graphene nanosheet can be established by calculating the temperature in each slab. The temperature gradient dT/dx is calculated from the linear fit of the temperature in

each slab.

A heat flux is introduced by continuously exchanging kinetic energy between the hottest atoms in the cold slab and the coldest atoms in the hot slab under NVE ensemble. The heat flux q can be written as[32]:

$$q = \frac{1}{2tA} \sum_{transfer} \frac{1}{2}(m_h v_h^{\ 2} - m_c v_c^{\ 2}) \tag{2}$$

where t is the total simulation time, A is the cross-sectional area perpendicular to the heat flux, m_h, m_c and v_h, v_c refer to the mass and velocity of the hottest atom in cold slab and the coldest atom in hot slab, respectively. The procedure of kinetic energy transferring is repeated every 50 time steps with a time step of 0.2 fs. The heat flux in PG reaches a dynamic steady state after 10^5 simulation time steps and a stable temperature profile appears in the PG (Figure 1b). The total energy transported across the system per unit cross-sectional area is also recorded, and an averaged heat flux q can be obtained from the slope of the curve plotted in Figure S1. Based on the calculated temperature gradient, the thermal conductivity of PG can be further determined by Fourier laws

$$k = q\left(\frac{dT}{dx}\right)^{-1} \tag{3}$$

3. Results & Discussion

The thermal conductivity of pristine single crystalline graphene is calculated using the described RNEMD method to verify the reliability of our computational settings. The atomistic structure of pristine graphene has a length of 20 nm and a width of 2.1 nm. Thermal conductivities along armchair and zigzag direction are calculated to be 109 and 123 W/mK, respectively, which show good agreement with the previously simulated

results of 89.6 and 92.3 W/mK by AIREBO potential[40]. And the average value between the two chiralities is also close to the reported results of 102 W/mK[44]. Moreover, our simulated thermal conductivity along the zigzag direction is larger than that along the armchair direction, which is also consistent with the reported dependence of thermal conductivity on chirality[14, 56]. However, the experimentally measured thermal conductivity of graphene is around 2500-5000 W/mK[11]. The difference between the experimental and computational results is because of the mismatch between mean free path of phonons in graphene (775 nm) and the length of our simulated system.[57] It has also been reported that the calculated thermal conductivity of graphene increases as the length of simulated system increases[58]. Admitting that the absolute simulated results are different from the experimental results, we focus on the qualitative dependence of κ on grain size, surface hydrogenation and in-plane strain.

The total energy transported across the system per unit cross-sectional area is recorded over the whole simulation process, as shown in Figure S1. The linear increase of total energy with the simulation time suggests a steady and time-independent heat flux q, i.e., the slope of the line. Figure 1b shows a typical temperature profile of PG. The temperature profile features several stages and jumps as the grain orientations and grain sizes change. Here, the temperature gradient of PG, dT / dx, is obtained by dividing the temperature interval ΔT by the simulation length interval Δx between hot and cold slab directly[51]. The effect of GB on thermal property can be effectively revealed by the temperature gradient, and the averaged thermal conductivity of the whole PG could be determined using Eq 3.

Moreover, we calculate the thermal conductivities of PG with different average grain sizes for further comparison. Figure S2a shows the atomistic structures of PG with average grain sizes of 200, 133, 100, 80, 67, 57, 50 nm^2, respectively. Here, the grain size is characterized by the averaged grain area since the polycrystalline models are constructed based on the predefined simulation size and number of grain using the Python code. The density of GB defects increases with the decrease in grain size with a fixed simulation size of 40 nm × 10 nm. Figure 1c plots the evolution of thermal conductivity with average grain size. It is noted that the thermal conductivity of PG increases with the average grain size. For a given average grain size, the thermal conductivity of PG may also be affected by the GB distributions and orientations. The thermal conductivity shown in Figure 1c represents the mean value obtained from several models with different GB distributions and orientations but the same average grain size, while the corresponding error bar shows the standard deviation of the results. The error bars are relatively small, implying that the thermal conductivity of PG has little dependence on the orientation and distribution of GBs. The agreement between our simulation results and the reported studies[33-35] also confirms the acceptance of the constructed PG models with different grain sizes.

Detailed analysis of the phonon density of states (PDOS) is carried out to elucidate the mechanism behind the dependence of thermal conductivity on grain size. PDOS analysis is widely adopted for nanoscale systems to evaluate the thermal characteristics qualitatively [55, 59-60]. In this paper, the variations of thermal conductivities obtained from MD simulations are verified by the PDOS of atoms. The PDOS is calculated by the

Fourier transform of atom velocity autocorrelation function at equilibrium[61]:

$$D(\omega) = \int_0^{\tau} \frac{\langle v(t)v(0)\rangle}{\langle v(0)v(0)\rangle} \exp(-i\omega t)dt \quad (4)$$

where ω is the frequency, v is the velocity of atoms, $\langle ... \rangle$ denotes time and atom number-averaged velocity autocorrelation function, τ is the time duration for calculation. Figure S2c shows the PDOS of the PG with different average grain sizes. It can be observed that the main peak of the PDOS shifts from low frequency domain to high frequency domain as the grain size increases. The blue shift of the main peak of PDOS is found in the reported investigations as well[33-34], which supports the accuracy of our simulation and analysis results. Moreover, the scattering of phonons at low frequency has been demonstrated as the intrinsic factor in the reduction of thermal conductivity[62]. A higher concentration of phonons at low frequency could slow down the phonon group velocities and restrict the mean free path[44], which results in larger thermal resistance.

3.1 In-plane strain dependent thermal conductivity of polycrystalline graphene

In order to modify the thermal conductivity of PG for potential applications, in-plane strains are applied along the direction of heat flux as illustrated in Figure 2a. Under periodic boundary condition, uniaxial strain can be achieved by changing the size of simulation box. The PG is stretched along *x*-direction at a strain rate of 0.01%/ps by scaling all atomic coordinates accordingly. Each stretching step is followed by a relaxation of 100 steps. Such procedure of stretching and relaxation is repeated at room temperature under NVT ensemble with time step τ = 0.1fs until the desired strain is archived. By studying the morphology of PG, we find that the planar geometry is

maintained under tensile strain while corrugation appears under compressive strain (Figure 2a). When the system reaches equilibrium after desired strain is applied, the RNEMD simulation is employed to obtain the thermal conductivity of PG.

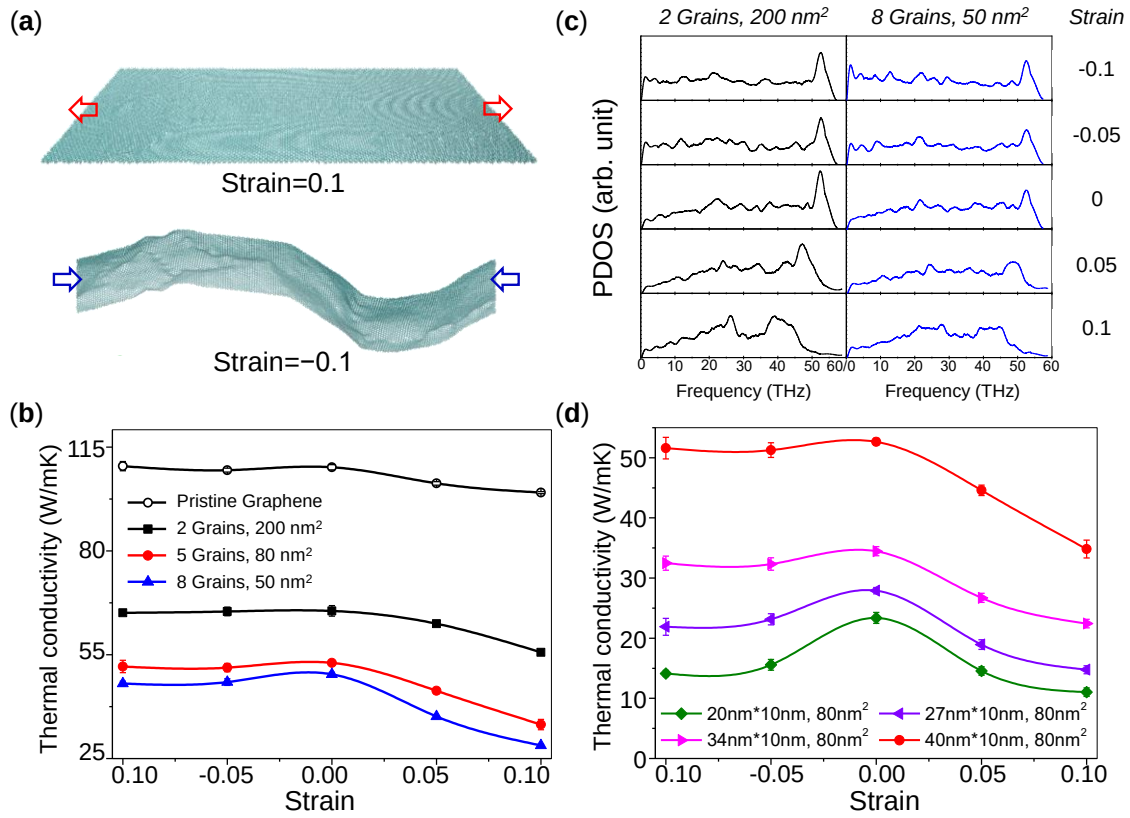

Figure 2. Thermal conductivity of polycrystalline graphene under different in-plane strains. (***a***) The morphological characteristics of polycrystalline graphene under strain ε = 0, 0.1 and −0.1. (***b***) Thermal conductivities of pristine graphene and polycrystalline graphene with average grain size of 200, 80 and 50 nm^2 under varying strains. (***c***) Phonon density of states of the atoms in polycrystalline graphene with average grain size of 200 and 50 nm^2 under varying strains. (*d*) Thermal conductivities of polycrystalline graphene with varying simulation sizes under the same average grain size 80 nm^2.

Figure 2b plots the simulated thermal conductivity of PG with average grain size being 200, 80, 50 nm^2 respectively. Thermal conductivity of all the considered PG models decreases remarkably with the tensile strain. The averaged deterioration of thermal conductivity is around 30% when the tensile strain reaches 0.1. What's more, the

decrease of thermal conductivity induced by tensile strain is more remarkable for the PG with smaller grain size. However, the thermal conductivity of PG is insensitive to the compressive strain. For all these simulated PG models, the change of thermal conductivity is less than 5% when the compressive strain reaches 0.1. Under same in-plane compression, the thermal conductivity of PG with smaller grains reduces more significantly compared to those with larger grains. For comparison, the thermal conductivities of pristine graphene along armchair direction under strain are calculated and plotted in Figure 2b. It is obvious that the reduction of thermal conductivity with tensile strain in PG is critical than that in pristine graphene. And the compressive strain causes little effect on the thermal conductivity. Similar strain dependency of thermal conductivity has been reported for the pristine graphene nanosheet[44]. Such relationship between thermal conductivity and tensile strain has also been noticed in literature[33].

Above results suggest that there is potential coupling effect between GBs and in-plane strain on thermal conductivity of graphene. Figure 2c shows the comparisons of PDOS for PG with an average grain size of 200 and 50 nm^2 under strain. For the PG with grain size of 200 nm^2, the G-peak is softened and shifts to the low-frequency domain gradually with the increasing tensile strain while another peak is developed at low-frequency domain. The red-shift and softening of G-peak indicate the energy decrease of the vibrational modes under tensile strain lead to the reduction of thermal conductivity. On the contrary, the compressive strain causes ignorable effects on the G-peak of PDOS. Red-shift of PDOS can be observed in the acoustic phonons, which leads to the slight decrease of thermal conductivity under compression. For the other PG

with grain size of 50 nm^2, the intensity of G-peak without strain is much less than that of PG with grain size of 200 nm^2. Similarly, the red-shift and softening of G-peak are shown in the PDOS of PG under tensile strain. The change of PDOS is more remarkable compared to that of the PG with larger grain size, which corresponds to the more notable decline of thermal conductivity. As compressive strain increases, the G-peak still stays at the same frequency and intensity while the red-shift in acoustic phonons becomes more critical. For the compressive strain at -0.1, several peaks are formed in acoustic phonons. Thus, more remarkable reduction of thermal conductivity under compressive strain is observed in the PG with smaller grain size. The comparison of PDOS for PG under tension and compression is consistent with the comparison of thermal conductivities described in Figure 2b.

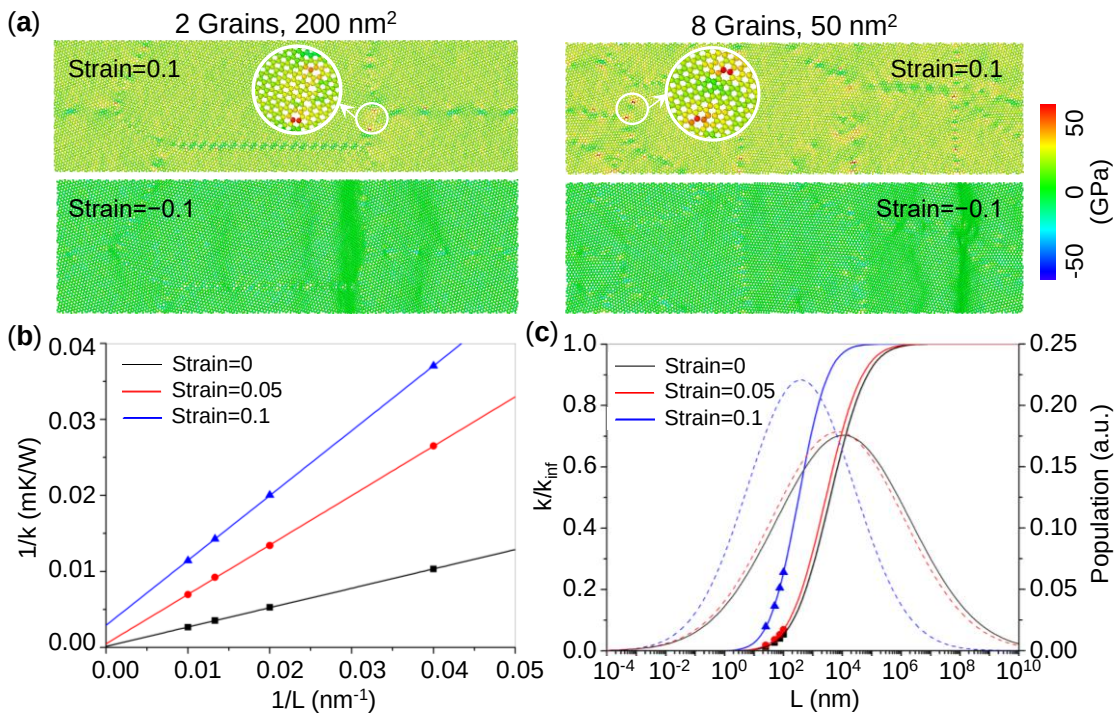

Figure 3. The analysis about the mechanisms of strain-dependent thermal conductivity from stress distribution and mean free math. (*a*) Comparisons between tensile stress contours for

polycrystalline graphene with average grain size being 200 nm^2 and 50 nm^2 under in-plane strain ε = 0.1 and −0.1. **(*b*)** Inverse of thermal conductivity 1/k as a function of the simulation length 1/L of pristine graphene with tensile strain ε = 0, 0.05 and 0.1. **(*c*)** Accumulation (full line) and distribution function of mean free path (dash line) for the pristine graphene samples with tensile strain ε = 0, 0.05 and 0.1.

To interpret the strain-dependent thermal conductivity, we further calculate the distributions of stress component σ_x, where x represents the loading direction of PG. The atomic stress of individual atoms in PG is calculated according to equation[63-64]

$$\sigma_{ij}^{\alpha} = \frac{1}{\Omega^{\alpha}}\left(\frac{1}{2}m^{\alpha}v_i^{\alpha}v_j^{\alpha} + \sum_{\beta=1,n} r_{\alpha\beta}^{j} f_{\alpha\beta}^{i}\right) \quad (5)$$

where i and j denote indices in Cartesian systems; α and β are the atomic indices; m^{α} and v^{α} denote the mass and velocity of atom α; $r_{\alpha\beta}$ is the distance between atoms α and β; Ω^{α} is the atomic volume of atom α. After obtaining the stress of each atom, the stress of the PG is computed by averaging over all the atoms in the sheet. The stress-strain curves of PG with varying grain size are plotted at Figure S3a, which show little difference between each other. The stress-strain curves of pristine graphene with armchair and zigzag orientations under tension are calculated for accuracy verification of our stress calculation, which are plotted in Figure S3b. The averaged Young's modulus and tensile strength extracted from the stress-strain curves are in good agreement with the experimental results[4] and the reported MD simulations based on the AIREBO potential[65].

Figure 3a shows the stress contours of σ_x for PG with average grain size being 133 nm^2 and 44 nm^2 under strain ε = 0.1 and −0.1. (More stress contours of PG are referred in SI at Figure S3c.) With the tensile strain applied, the average stress in PG increases, which is also shown in the stress-strain curves of Figure S3a. More remarkably, distinctly

high stress concentration at the GBs can be observed in PG under tensile strain. The localization of stress field arising from GB defects has been reported to reduce the interfacial thermal conductance in hybrid graphene and hexagon boron nitride in a previous study[66]. By comparing with that study, we conclude that the average stress in PG weakens the overall thermal conductivity and stress concentration at the GB defects stimulates the phonon scattering which contribute as one of the factors for the difference between the decrease of thermal conductivity in PG with varying grain size under tension. As the grain size decreases, more defects with stress concentration serve as the phonon scattering centers due to the higher density of GBs, which lead to more decline in thermal conductivity.

The mechanism behind the effect of stress on thermal conductivity is further evaluated by simulating pristine graphene samples with varying simulated lengths under in-plane strain ε = 0, 0.05 and 0.1. As the tensile strain increases, the tensile stress on each atom increases. The length-dependent thermal conductivity of graphene has been demonstrated in several experimental and theoretical studies[67-69], which can be described with the following linear function between inverse of thermal conductivity k versus the inverse of the system length L[70]:

$$\frac{1}{k}=\frac{1}{k_{\text{inf}}}\left(1+\frac{\lambda}{L}\right) \tag{6}$$

Eq 6 gives the convergent bulk thermal conductivity k_{inf} of the graphene using infinite size, and the parameter λ denotes the characteristic length of system. Accordingly, the linear correlations between the $1/k$ and $1/L$ can be observed in graphene for strain values of ε = 0, 0.05 and 0.1, as shown in Figure 3b. By simulating the k of PG with lengths of

25, 50, 75 and 100 nm under different strain ε = 0, 0.05 and 0.1, the values of k_{inf} and λ under each strain can be determined from the linear fit of the simulated k as listed in Table 1. For the graphene without applied strain, the k_{inf} is obtained as 6974 W/mK by Eq 6, which agrees with the experimental results (2500-5000 W/mK). For graphene under ε = 0.05 and 0.1, the k_{inf} values, which decrease with the increase of tensile strain, are determined to be 2065 and 341 W/mK, respectively.

Table 1. The estimated expectation μ and variance σ^2 of the phonon spectrum using Eq 9 based on the fitting parameters k_{inf} and λ as plotted in Figure 3b, and the corresponding average mean free path L_{MFP} for the pristine graphene samples with tensile strain ε = 0, 0.05 and 0.1.

Tensile Strain	k_{inf} (W/mK)	λ (nm)	μ (nm)	σ^2	L_{MPF} (nm)
0	6974	1777	0.782	5.155	10757
0.05	2065	1342	0.721	4.997	7051
0.1	341	291	0.122	3.264	385

After obtaining k_{inf} and λ, the spectral contribution of phonons to the thermal conductivity can be established by an accumulation function[71-72]:

$$\frac{k(\alpha)}{k_{\text{inf}}} = \int_0^{\alpha} f(\tilde{\alpha}) d\tilde{\alpha} \tag{7}$$

where $f(\alpha)$ is the distribution function of the mean free path (MFP) of dominating phonons and α is the natural logarithm of the dimensionless simulation length L/λ ($\alpha = \log\left(\frac{L}{\lambda}\right)$). Here, a normal distribution is assumed for the expression of $f(\alpha)$ following a reported study[72]:

$$f(\alpha) = \frac{1}{\sigma\sqrt{2\pi}} \exp\left(-\frac{(\alpha-\mu)^2}{2\sigma^2}\right) \tag{8}$$

The expectation μ and variance σ^2 can be estimated by fitting the accumulation of thermal conductivity as a function of simulation length L:

$$\frac{k(\alpha)}{k_{\inf}} = \frac{1}{2}\left[1 + erf\left(\frac{\alpha - \mu}{\sigma\sqrt{2}}\right)\right] \tag{9}$$

Finally, the average MFP of the system can be calculated from the value of μ as the relationship $L_{MPF} = \lambda \cdot 10^{\mu}$.

Figure 3c shows the fitting accumulation function (full line) for graphene system under varying strain ε = 0, 0.05 and 0.1. The corresponding normal distributions are also illustrated in Figure 3c with the fitting parameters and average MFP listed in Table 1. The average MFP in graphene without applied strain is estimated to be 10757 nm. While the graphene under strains of 0.05 and 0.1 have much shorter MFPs of 7051 and 385 nm, respectively. Since the data points are distributed unevenly through the overall range of L, the absolute value of estimated MFP is not in good agreement with the experimental results (775 nm). Thus, as stated before, we focus qualitatively on the relationships among the MFPs of graphene under different strains instead. A significant suppression of the MFP of graphene system caused by tensile stress is indicated from the comparisons. According to the classical lattice thermal transport theory[73], the thermal conductivity is proportional to the MFP:

$$k = \sum_m C_v v_m l \tag{10}$$

where m denotes the phonon mode occupied at a specific temperature; C_v, v_m and l denote the specific heat, group velocity and MFP, respectively. Eq 10 clearly implies that PG with shorter MFP corresponds to lower thermal conductivity. Additionally, the MFP decrease rapidly with the tensile strain, which facilitates the deterioration of thermal

conductivity. As a consequence, the PG exhibits lower thermal conductivity when the tensile strain becomes larger. It reveals that the tensile stress on atoms weakens the MFP of system and results in the decline of thermal conductivity. And that more severe stress state of atoms will act as phonon scattering centers and aggravate the deterioration of thermal conductivity, like the stress concentration on GBs as Figure 3a shows. Therefore, it can be demonstrated that PG with smaller average grain size, which have larger GB defect density, exhibit more decline of thermal conductivity with tensile strain. Since the proportion of atoms with stress concentration is small to all atoms in PG, the differences between the reduction of thermal conductivity in PG with varying grain sizes are relatively small but still exists.

For PG under compression, the stress distributions are uniform without concentration, which is similar to that of the PG without strain applied (Figure 3a). As the compressive strain increases, the stress field on PG changes a little, and so does the thermal conductivity, which states that varying compressive stress contributes only slightly to change in conductivity of PG. It can be attributed to the unique 2D atomic monolayer structure of graphene that can release the stress by out-of-plane deformation. The stress concentration caused by the strain mismatch at GB defects also vanishes by the formation of corrugations on GBs under compression, as illustrated in Figure 2a. However, the corrugations on graphene has been already reported to cause the phonon scattering and provide barrier to the thermal transport[17, 74]. An inspiring study by Yashashree Kulkarni *et al.* has investigated the coupled strain and size dependence of the thermal conductance of GB in graphene and revealed the important effect of the

geometric instability of GB on the thermal transport across the GB[75]. Thus, it is confusing that the compressive strain causes negligible decline in the thermal conductivity of PG with simulation size of 40 nm*10 nm as plotted in Figure 2b. The independence of thermal conductivity on compressive strain has also been observed in the single crystal graphene as well[44].

In order to study the abnormal compression-insensitive thermal conductivity, we further investigate the thermal conductivity of PG with different simulation sizes under strains that possesses the same average grain size of 67 nm^2. The results are shown in Figure 2d. The thermal conductivity of PG still falls with the applied tensile strain. Noticeably, more significant drop of thermal conductivity with compressive strain can be observed for PG with smaller simulation size. For PG with simulation size of 20 nm * 10 nm, the decline of thermal conductivity exceeds even 35% when the compressive strain reaches 0.1, which is much larger than that for PG with simulation size of 40 nm * 10 nm. It indicates that the observed effect of corrugations caused by compression on the thermal conductivity of PG depends on the simulation size. Note that when simulation size of PG is small, the scattering of phonons on the corrugations will prominently influence the thermal conductivity of the PG, but the effect will become weaker with increasing simulation size. For PG with parallel twin grain boundaries, the thermal conductivity k can be described as the equation proposed by Akbar Bagri *et al.*[32]:

$$\frac{1}{k} = \frac{1}{k_g} + \frac{1}{GL} \tag{11}$$

where k_g is the thermal conductivity of graphene grains, G is the interfacial conductance (Kapitza conductance) of GB with corrugations, and L is the simulation length. Since the

corresponding theoretical models for PG with random distributions and orientations of GBs has not been established completely, we try to use the Eq 11 to evaluate the relationship between interfacial conductance of GB and thermal conductivity of PG qualitatively, and demonstrate that the important role of simulation size in the dependence of thermal conductivity on compressive strains. The compression changes the micromorphology characteristics of corrugations on GBs, which leads to the change of interfacial conductance G[17]. According to Eq 11, the variation of G causes negligible change to the thermal conductivity when the size is large. The prediction of Eq 11 agrees with the simulated results shown in Figure 2b and Figure 2d well. The similar coupling size and strain effect on the thermal property in 2D nano-material has been also reported at the previous study by Yashashree Kulkarni *et al*[75]. It indicates the thermal conductance of GB in graphene becomes insensitive to the compressive strain beyond certain aspect ratio of the simulation cells due to less buckling structures in GB, which can support our results of the thermal conductivities of PG.

Thus, we find that the strain-dependent thermal property of PG is closely related to the stress field and the corrugations due to GBs. The mechanisms behind the effect of tensile stress are also uncovered by the analysis from PDOS and MFP. Additionally, the effect introduced by the simulation size on the thermal conductivity of PG under compression is investigated.

3.2 Thermal conductivity of surface hydrogenated polycrystalline graphene under in-plane strain

After the discussion on strain dependent thermal conductivity of PG, surface

hydrogenated PGs are constructed to investigate the coupling effect of in-plane strain and surface functionalization on thermal conductivity. First principle calculations have revealed that GB is energetically favorable place for adatoms[42], thus the constructed hydrogenated PG has hydrogen atoms bonded with carbon atoms on GBs. This preference continues until reaching saturation on GBs, after which hydrogen atoms permeate randomly on other regions within the pristine graphene grains. The hydrogenation coverage (H-coverage) varies from 0 (graphene) to 100% (graphane). Figure 4a shows the atomistic structures of typical hydrogenated PG with different H-coverages. We can find that carbon atoms on GBs are fully hydrogenated under H-coverage=10%. The adsorption of hydrogen atoms mainly occurs on GBs with H-coverage from 0 to 10%. When H-coverage exceeds 10%, hydrogenation at the GB is saturated and the hydrogen atoms are spread randomly on remaining pristine grains.

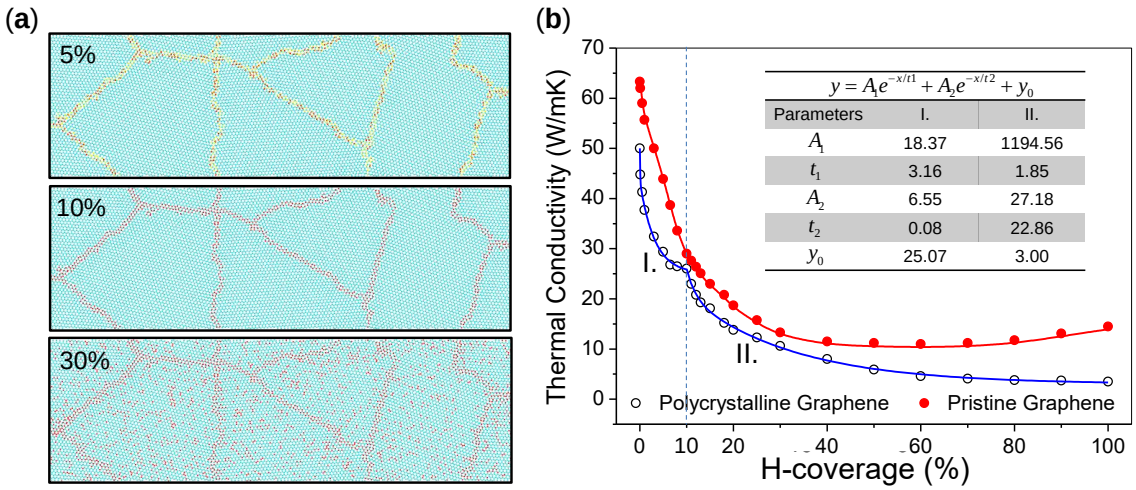

Figure 4. The surface hydrogenation dependent thermal conductivities of polycrystalline graphene with average grain size 57 nm². (***a***) The atomistic structure of hydrogenated polycrystalline graphene. The hydrogen atoms are absorbed on the carbon atoms on GBs at first. After reaching saturation on GBs, the hydrogen atoms are spread randomly on remaining pristine grains. The regions in yellow are GBs. Hydrogen atoms are colored in red while the carbon atoms are colored in cyan. (***b***) The comparison between the surface hydrogenation dependent thermal conductivities of

polycrystalline graphene and pristine graphene. The stage-1 and stage-2 of the hydrogenated polycrystalline graphene are fitted. The inset is the format of fitting exponential function and the corresponding fitting parameters.

The calculated thermal conductivities of hydrogenated PG with varying H-coverages are plotted in Figure 4b (the blue line and points). It shows that hydrogenation significantly reduces the thermal conductivity of PG, which results from the remarkable softening of G-band of the phonon spectra by hydrogenation, as shown in Figure S4. However, it is noticeable that the decrease of thermal conductivity with the increase of H-coverage shows an unexpected two-stages evolution. When H-coverage increases from 0 to 10%, the decrease of thermal conductivity is drastic and then slows down when hydrogenation on GB reaches saturation. With the further increase of H-coverage from 10% to 100%, the thermal conductivity declines rapidly again and converges to a stable state gradually. It suggests that the thermal conductivity of PG changes by only a little when the GBs are close to be fully hydrogenated (at the H-coverage of 10%), even though the H-coverage still increases. The hydrogenation on GBs delays the sharp decline of thermal conductivity of PG. When hydrogenation reaches saturation on GBs, further hydrogenation occurs at random locations inside the grains of PG, where the increase in H-coverage leads to a second rapid drop of thermal conductivity. After H-coverage exceeds 60%, the thermal conductivity of hydrogenated PG becomes insensitive to the coverage. As the Figure 4b shows, the conductivity in both stage-1 and stage-2 follow a similar exponential decay with H-coverage increase. The fitting functions with parameters can be referred in Figure 4b. Also, the remarkable transition between two stages can be observed from the fitting curves.

For more comparisons, we calculate the thermal conductivities of single crystalline graphene with hydrogenation. The calculated thermal conductivities of single crystalline graphene with H-coverages varying from 0 to 100% are also illustrated in Figure 4b (the red line). It is noticed that the thermal conductivity decreases rapidly with increasing H-coverage up to ~30%, and then remains almost insensitive to the coverage beyond the limit, finally undergoes a small increase near 100% H-coverage. The effect of hydrogenation on thermal conductivity of pristine graphene is similar with the reported results[40]. The thermal conductivities of pristine graphene under hydrogenation have only one stage, which is quite different from that of PG. It can be concluded that the GBs have essential effects on the sensitivity of thermal conductivity to hydrogenation. Further, we notice that the thermal conductivity of PG is close to the value of pristine graphene under the same H-coverage when hydrogenation on GB reaches saturation at ~10%. It is well known that the introduction of GB defects causes the decline of thermal conductivity of graphene[55]. However, the negative effects by GB is weakened significantly here when the GBs in PG are fully hydrogenated. The beneficial suppression of negative effect by GB on thermal conductivity using surface hydrogenation provides a possible route for the manipulation of graphene thermal conductivity in carbon-based nanodevices.

In our previous study, thermal conductivity of graphene nanoribbon was demonstrated to be tunable by manipulating the geometrical characteristics of graphane domains without changing the amount of hydrogenation[51]. It was revealed that graphane domains with larger circumferences and more dispersed arrangements have more negative effects on heat transfer due to the scattering of phonons occurring at the

graphene-graphane interface, which results in the lower thermal conductivity of graphene nanoribbon. Moreover, the effect of circumference on thermal conductivity can be used to interpret the observed two-stage variation of conductivity. Since hydrogen atoms have preference to fill the GBs, the full hydrogenation on GBs can be regarded as complete graphene domains interspersed with strip profiles of graphane. The growth of the circumference of graphane domains slows down when the GBs approaches saturation with hydrogen atoms, which leads to the stable thermal conductivities at the end of stage-1. On the contrary, we suppose that random hydrogenation can be treated as a special hydrogenation case consisting of numerous tiny graphane domains that are randomly dispersed. Once the hydrogen atoms overflow from the GBs, the random distribution causes a rapid increase of circumference, which is related with the sharp drop of the thermal conductivity at the beginning of stage-2. From the perspective of graphane-graphene interface and circumference of graphane domains, the surface hydrogenation dependent thermal conductivity of PG can be interpreted qualitatively. More theoretical and in-depth analyses are expected further.

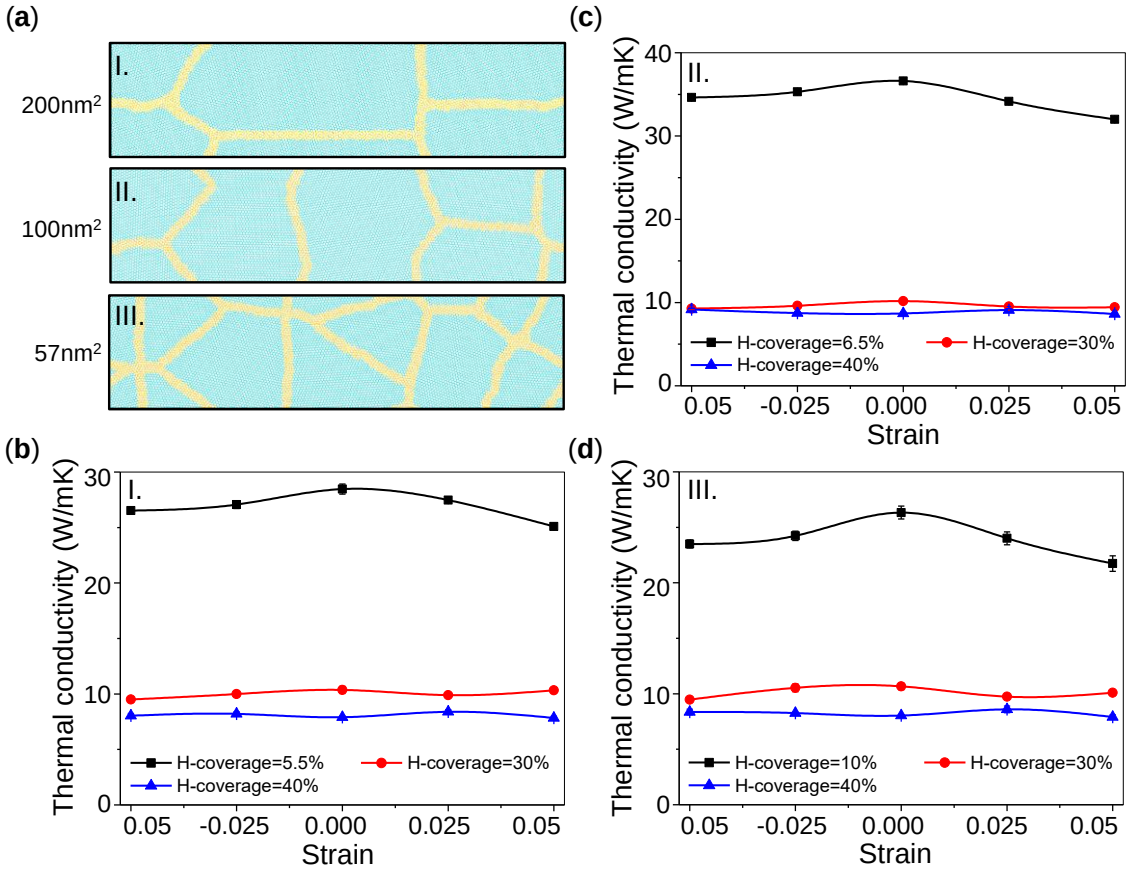

Figure 5. Strain dependent thermal conductivity of hydrogenated polycrystalline graphene. (***a***) Atomistic structures of polycrystalline graphene with averaged grain size of 200, 100 and 57 nm^2. (***b-d***) Strain dependent thermal conductivities of hydrogenated polycrystalline graphene with average grain size of 200, 100 and 57 nm^2 under varying H-coverage, respectively. The critical H-coverages where GBs are hydrogenated completely are 5.5%, 6.5%, and 10%, respectively.

Further we also apply the in-plane strain on the hydrogenated PG to investigate how the hydrogenation affects the strain dependent thermal conductivity of PG. The PG with average grain size of 200, 100, 57 nm^2 are considered, as the Figure 5a shown. The calculated thermal conductivities are plotted in Figure 5b,c, respectively. It can be observed that the hydrogenation brings noticeable impacts on the sensitivity of thermal conductivity to the strain, which shows similarity among PG with different average grain sizes. For the lower H-coverage, the thermal conductivity of hydrogenated PG decreases

with the tensile and compressive strain, which is still similar with the variation of PG without hydrogenation shown above. While the thermal conductivity of PG becomes insensitive to the in-plane strain under the higher H-coverage. As the Figure 5b,c shown, the thermal conductivities of PG with average grain size of 200, 100, 57 nm^2 remain almost unchanged with the tensile and compressive strain, under H-coverage of 30% and 40%. The coupling effects of hydrogenation and strain on the thermal conductivity of PG is revealed.

4. Conclusions

In summary, the thermal characteristics of polycrystalline graphene have been studied systematically using molecular dynamics simulations. In order to effectively manipulate the thermal properties, the effect of surface hydrogenation and in-plane strain on the thermal conductivity due to the presence of GBs are revealed. We find that the thermal conductivity of PG is tunable under in-plane strains. The thermal conductivity decreases with the increase of tensile strain. PG with coarse grains possesses higher thermal conductivity, and graphene with fine grains shows more severe deterioration than that with coarse grains with increasing tensile strain. The detailed analyses from the perspectives of classical lattice thermal transport theory and phonon vibrational spectra are performed to demonstrate the soften of phonon modes in nanocrystalline graphene. Further MFP analysis reveals that the mechanism of the tensile strain-dependent thermal conductivity is attributed to the change of stress distributions under applied in-plane strain. For PG under compression, the effect of strain on thermal conductivity is sensitive to the simulation size. More significant decline of thermal conductivity with increasing

compressive strain can be observed for PG with smaller simulation size. As the size increases, the GBs have less dominating influence in the thermal transport, which results in a less significant decline. Additionally, the effects of surface hydrogenation on thermal conductivity of PG are investigated. An extraordinary dependence of thermal conductivity on H-coverage with unexpected two stages is observed, which is interpreted preliminarily from the circumference and arrangement of graphane domains. The negative effect of GB on the thermal conductivity is weakened significantly under full hydrogenation. Moreover, the coupling effects of hydrogenation and strain on the thermal conductivity of PG is revealed. The thermal conductivity of PG is insensitive to the in-plane strain under higher H-coverage. Such tunable thermal characteristics of PG pave the way for the design of graphene-based nano-sensors and flexible nanodevices. Our results provide useful inspiration for the practical applications of graphene. Further theoretical simulations about out-of-plane thermal characteristics and experimental verifications of our prediction are also expected.

Supporting Information

The total energy transported across the system per unit cross-sectional area over the whole simulation process. Comparisons between thermal conductivities of PG with different average grain sizes. Stress-strain curves of PG with different average grain sizes under tensile strain to 0.1, stress-strain curves of pristine graphene with armchair and zigzag orientations till failure and tensile stress contours for PG with average grain size of 80 nm^2 under in-plane strain $\varepsilon = 0, 0.1, -0.1$. Phonon density of states of the atoms in

PG with varying surface hydrogenations.

Acknowledgements

We gratefully acknowledge the support of the National Natural Science Foundation of China (No. 11402145), the Open Fund of IPOC (BUPT) (No. IPOC2017B009) and the Medical-Engineering Cross Fund of Shanghai Jiao Tong University (YG2015MS13, YG2017QN64). The computational support for this work was provided by Center for HPC, Shanghai Jiao Tong University.

References

1. Boukhvalov, D. W.; Katsnelson, M. I. Chemical Functionalization of Graphene. *Journal of Physics: Condensed Matter* **2009**, *21*, 344205.

2. Salehi-Khojin, A.; Estrada, D.; Lin, K. Y.; Ran, K.; Haasch, R. T.; Zuo, J.-M.; Pop, E.; Masel, R. I. Chemical Sensors Based on Randomly Stacked Graphene Flakes. *Applied Physics Letters* **2012**, *100*, 033111.

3. Zhang, Y.; Tan, Y.-W.; Stormer, H. L.; Kim, P. Experimental Observation of the Quantum Hall Effect and Berry's Phase in Graphene. *Nature* **2005**, *438*, 201-204.

4. Lee, C.; Wei, X.; Kysar, J. W.; Hone, J. Measurement of the Elastic Properties and Intrinsic Strength of Monolayer Graphene. *science* **2008**, *321*, 385-388.

5. Boukhvalov, D.; Katsnelson, M.; Lichtenstein, A. Hydrogen on Graphene: Electronic Structure, Total Energy, Structural Distortions and Magnetism from First-Principles Calculations. *Physical Review B* **2008**, *77*, 035427.

6. Singh, V.; Joung, D.; Zhai, L.; Das, S.; Khondaker, S. I.; Seal, S. Graphene Based Materials: Past, Present and Future. *Progress in materials science* **2011**, *56*, 1178-1271.

7. Soldano, C.; Mahmood, A.; Dujardin, E. Production, Properties and Potential of Graphene. *Carbon* **2010**, *48*, 2127-2150.

8. Neto, A. C.; Guinea, F.; Peres, N.; Novoselov, K. S.; Geim, A. K. The Electronic Properties of Graphene. *Reviews of modern physics* **2009**, *81*, 109.

9. Geim, A. K.; Novoselov, K. S. The Rise of Graphene. *Nature materials* **2007**, *6*, 183-191.

10. Balandin, A. A. Thermal Properties of Graphene and Nanostructured Carbon Materials. *Nat Mater* **2011**, *10*, 569-581.

11. Balandin, A. A.; Ghosh, S.; Bao, W.; Calizo, I.; Teweldebrhan, D.; Miao, F.; Lau, C.

N. Superior Thermal Conductivity of Single-Layer Graphene. *Nano Lett.* **2008**, *8*, 902-907.

12. Cai, W.; Moore, A. L.; Zhu, Y.; Li, X.; Chen, S.; Shi, L.; Ruoff, R. S. Thermal Transport in Suspended and Supported Monolayer Graphene Grown by Chemical Vapor Deposition. *Nano letters* **2010**, *10*, 1645-1651.

13. Evans, W. J.; Hu, L.; Keblinski, P. Thermal Conductivity of Graphene Ribbons from Equilibrium Molecular Dynamics: Effect of Ribbon Width, Edge Roughness, and Hydrogen Termination. *Applied Physics Letters* **2010**, *96*, 203112.

14. Zhong, W.-R.; Zhang, M.-P.; Ai, B.-Q.; Zheng, D.-Q. Chirality and Thickness-Dependent Thermal Conductivity of Few-Layer Graphene: A Molecular Dynamics Study. *Applied Physics Letters* **2011**, *98*, 113107.

15. Jiang, J.-W.; Wang, J.-S.; Li, B. Thermal Conductance of Graphene and Dimerite. *Physical Review B* **2009**, *79*, 205418.

16. Wang, H.; Hu, S.; Takahashi, K.; Zhang, X.; Takamatsu, H.; Chen, J. Experimental Study of Thermal Rectification in Suspended Monolayer Graphene. *Nature Communications* **2017**, *8*, 15843.

17. Li, Y.; Wei, A.; Datta, D. Thermal Characteristics of Graphene Nanoribbons Endorsed by Surface Functionalization. *Carbon* **2017**, *113*, 274-282.

18. Yan, Z.; Liu, G.; Khan, J. M.; Balandin, A. A. Graphene Quilts for Thermal Management of High-Power Gan Transistors. *Nature Communications* **2012**, *3*, 827.

19. Renteria, D. J.; Nika, L. D.; Balandin, A. A. Graphene Thermal Properties: Applications in Thermal Management and Energy Storage. *Applied Sciences* **2014**, *4*, 525-547.

20. Choy, K. Chemical Vapour Deposition of Coatings. *Progress in materials science* **2003**, *48*, 57-170.

21. Tietjen, J. J. Chemical Vapor Deposition of Electronic Materials. *Annual Review of Materials Science* **1973**, *3*, 317-326.

22. Kim, K.; Lee, Z.; Regan, W.; Kisielowski, C.; Crommie, M.; Zettl, A. Grain Boundary Mapping in Polycrystalline Graphene. *ACS nano* **2011**, *5*, 2142-2146.

23. Huang, P. Y.; Ruiz-Vargas, C. S.; van der Zande, A. M.; Whitney, W. S.; Levendorf, M. P.; Kevek, J. W.; Garg, S.; Alden, J. S.; Hustedt, C. J.; Zhu, Y. Grains and Grain Boundaries in Single-Layer Graphene Atomic Patchwork Quilts. *Nature* **2011**, *469*, 389-392.

24. Li, Y.; Datta, D.; Li, Z. Anomalous Mechanical Characteristics of Graphene with Tilt Grain Boundaries Tuned by Hydrogenation. *Carbon* **2015**, *90*, 234-241.

25. Grantab, R.; Shenoy, V. B.; Ruoff, R. S. Anomalous Strength Characteristics of Tilt Grain Boundaries in Graphene. *Science* **2010**, *330*, 946-948.

26. Wei, A.; Li, Y.; Datta, D.; Guo, H.; Lv, Z. Mechanical Properties of Graphene Grain Boundary and Hexagonal Boron Nitride Lateral Heterostructure with Controlled Domain Size. *Computational Materials Science* **2017**, *126*, 474-478.

27. Li, Y.; Wei, A.; Ye, H.; Yao, H. Mechanical and Thermal Properties of Grain Boundary in a Planar Heterostructure of Graphene and Hexagonal Boron Nitride. *Nanoscale* **2018**, *10*, 3497-3508.

28. Tsen, A. W.; Brown, L.; Levendorf, M. P.; Ghahari, F.; Huang, P. Y.; Havener, R. W.; Ruiz-Vargas, C. S.; Muller, D. A.; Kim, P.; Park, J. Tailoring Electrical Transport across Grain Boundaries in Polycrystalline Graphene. *Science* **2012**, *336*, 1143.

29. Kaplan-Ashiri, I.; Cohen, S. R.; Gartsman, K.; Ivanovskaya, V.; Heine, T.; Seifert, G.; Wiesel, I.; Wagner, H. D.; Tenne, R. On the Mechanical Behavior of Ws2 Nanotubes under Axial Tension and Compression. *Proceedings of the National Academy of Sciences of the United States of America* **2006**, *103*, 523-528.

30. Hall, E. O. The Deformation and Ageing of Mild Steel: Iii Discussion of Results. *Proceedings of the Physical Society. Section B* **1951**, *64*, 747.

31. Tang, D.-M.; Ren, C.-L.; Wei, X.; Wang, M.-S.; Liu, C.; Bando, Y.; Golberg, D. Mechanical Properties of Bamboo-Like Boron Nitride Nanotubes by in Situ Tem and Md Simulations: Strengthening Effect of Interlocked Joint Interfaces. *ACS Nano* **2011**, *5*, 7362-7368.

32. Bagri, A.; Kim, S.-P.; Ruoff, R. S.; Shenoy, V. B. Thermal Transport across Twin Grain Boundaries in Polycrystalline Graphene from Nonequilibrium Molecular Dynamics Simulations. *Nano letters* **2011**, *11*, 3917-3921.

33. Wu, P.; Quek, S.; Sha, Z.; Dong, Z.; Liu, X.; Zhang, G.; Pei, Q.; Zhang, Y. Thermal Transport Behavior of Polycrystalline Graphene: A Molecular Dynamics Study. *Journal of applied physics* **2014**, *116*, 204303.

34. Mortazavi, B.; Potschke, M.; Cuniberti, G. Multiscale Modeling of Thermal Conductivity of Polycrystalline Graphene Sheets. *Nanoscale* **2014**, *6*, 3344-3352.

35. Liu, H.; Lin, Y.; Luo, S. Grain Boundary Energy and Grain Size Dependences of Thermal Conductivity of Polycrystalline Graphene. *The Journal of Physical Chemistry C* **2014**, *118*, 24797-24802.

36. Li, G.; Li, Y.; Liu, H.; Guo, Y.; Li, Y.; Zhu, D. Architecture of Graphdiyne Nanoscale Films. *Chemical Communications* **2010**, *46*, 3256-3258.

37. Zhou, J.; Wang, Q.; Sun, Q.; Chen, X.; Kawazoe, Y.; Jena, P. Ferromagnetism in Semihydrogenated Graphene Sheet. *Nano letters* **2009**, *9*, 3867-3870.

38. Sofo, J. O.; Chaudhari, A. S.; Barber, G. D. Graphane: A Two-Dimensional Hydrocarbon. *Physical Review B* **2007**, *75*, 153401.

39. Elias, D. C.; Nair, R. R.; Mohiuddin, T.; Morozov, S.; Blake, P.; Halsall, M.; Ferrari, A.; Boukhvalov, D.; Katsnelson, M.; Geim, A. Control of Graphene's Properties by

Reversible Hydrogenation: Evidence for Graphane. *Science* **2009**, *323*, 610-613.

40. Pei, Q.-X.; Sha, Z.-D.; Zhang, Y.-W. A Theoretical Analysis of the Thermal Conductivity of Hydrogenated Graphene. *Carbon* **2011**, *49*, 4752-4759.

41. Chien, S.-K.; Yang, Y.-T.; Chen, C. o.-K. Influence of Hydrogen Functionalization on Thermal Conductivity of Graphene: Nonequilibrium Molecular Dynamics Simulations. *Applied Physics Letters* **2011**, *98*, 033107.

42. Malola, S.; Häkkinen, H.; Koskinen, P. Structural, Chemical, and Dynamical Trends in Graphene Grain Boundaries. *Physical Review B* **2010**, *81*, 165447.

43. Mu, X.; Song, Z.; Wang, Y.; Xu, Z.; Go, D. B.; Luo, T. Thermal Transport in Oxidized Polycrystalline Graphene. *Carbon* **2016**, *108*, 318-326.

44. Wei, N.; Xu, L.; Wang, H.-Q.; Zheng, J.-C. Strain Engineering of Thermal Conductivity in Graphene Sheets and Nanoribbons: A Demonstration of Magic Flexibility. *Nanotechnology* **2011**, *22*, 105705.

45. Wei, Y.; Wu, J.; Yin, H.; Shi, X.; Yang, R.; Dresselhaus, M. The Nature of Strength Enhancement and Weakening by Pentagon–Heptagon Defects In graphene. *Nat Mater* **2012**, *11*, 759-763.

46. Müller-Plathe, F.; Bordat, P. Reverse Non-Equilibrium Molecular Dynamics. In *Novel Methods in Soft Matter Simulations*; Karttunen, M., Lukkarinen, A., Vattulainen, I., Eds.; Springer: Berlin, Heidelberg, 2004; pp 310-326.

47. Plimpton, S. Fast Parallel Algorithms for Short-Range Molecular Dynamics. *Journal of computational physics* **1995**, *117*, 1-19.

48. Stuart, S. J.; Tutein, A. B.; Harrison, J. A. A Reactive Potential for Hydrocarbons with Intermolecular Interactions. *The Journal of chemical physics* **2000**, *112*, 6472-6486.

49. Ng, T.; Yeo, J.; Liu, Z. A Molecular Dynamics Study of the Thermal Conductivity of Graphene Nanoribbons Containing Dispersed Stone–Thrower–Wales Defects. *Carbon* **2012**, *50*, 4887-4893.

50. Wu, J.; Wei, Y. Grain Misorientation and Grain-Boundary Rotation Dependent Mechanical Properties in Polycrystalline Graphene. *Journal of the Mechanics and Physics of Solids* **2013**, *61*, 1421-1432.

51. Wei, A.; Li, Y.; Li, Y.; Ye, H. Thermal Characteristics of Graphene Nanosheet with Graphane Domains of Varying Morphologies. *Computational Materials Science* **2017**, *138*, 192-198.

52. Shekhawat, A.; Ritchie, R. O. Toughness and Strength of Nanocrystalline Graphene. *Nature Communications* **2016**, *7*, 10546.

53. Ophus, C.; Shekhawat, A.; Rasool, H.; Zettl, A. Large-Scale Experimental and Theoretical Study of Graphene Grain Boundary Structures. *Physical Review B* **2015**, *92*, 205402.

54. Huang, Y.; Wu, J.; Hwang, K. Thickness of Graphene and Single-Wall Carbon Nanotubes. *Physical review B* **2006**, *74*, 245413.

55. Mortazavi, B.; Ahzi, S. Thermal Conductivity and Tensile Response of Defective Graphene: A Molecular Dynamics Study. *Carbon* **2013**, *63*, 460-470.

56. Lukes, J. R.; Zhong, H. Thermal Conductivity of Individual Single-Wall Carbon Nanotubes. *Journal of Heat Transfer* **2006**, *129*, 705-716.

57. Ghosh, S.; Calizo, I.; Teweldebrhan, D.; Pokatilov, E.; Nika, D.; Balandin, A.; Bao, W.; Miao, F.; Lau, C. N. Extremely High Thermal Conductivity of Graphene: Prospects for Thermal Management Applications in Nanoelectronic Circuits. *Applied Physics Letters* **2008**, *92*, 151911.

58. Guo, Z.; Zhang, D.; Gong, X.-G. Thermal Conductivity of Graphene Nanoribbons. *Applied physics letters* **2009**, *95*, 163103.

59. Zhiping, X.; Markus, J. B. Strain Controlled Thermomutability of Single-Walled Carbon Nanotubes. *Nanotechnology* **2009**, *20*, 185701.

60. Xu, L.; Zhang, X.; Zheng, Y. Local Strain Effect on the Thermal Transport of Graphene Nanoribbons: A Molecular Dynamics Investigation. *Physical Chemistry Chemical Physics* **2015**, *17*, 12031-12040.

61. Hirata, Y. Molecular Dynamics Simulation Study of the Rotational and Translational Motions of Liquid Acetonitrile. *The Journal of Physical Chemistry A* **2002**, *106*, 2187-2191.

62. Ghosh, S.; Bao, W.; Nika, D. L.; Subrina, S.; Pokatilov, E. P.; Lau, C. N.; Balandin, A. A. Dimensional Crossover of Thermal Transport in Few-Layer Graphene. *Nat Mater* **2010**, *9*, 555-558.

63. Basinski, Z. S.; Duesbery, M. S.; Taylor, R. Influence of Shear Stress on Screw Dislocations in a Model Sodium Lattice. *Canadian Journal of Physics* **1971**, *49*, 2160-2180.

64. Chandra, N.; Namilae, S.; Shet, C. Local Elastic Properties of Carbon Nanotubes in the Presence of Stone-Wales Defects. *Physical Review B* **2004**, *69*, 094101.

65. He, L.; Guo, S.; Lei, J.; Sha, Z.; Liu, Z. The Effect of Stone–Thrower–Wales Defects on Mechanical Properties of Graphene Sheets – a Molecular Dynamics Study. *Carbon* **2014**, *75*, 124-132.

66. Liu, X.; Zhang, G.; Zhang, Y.-W. Topological Defects at the Graphene/H-Bn Interface Abnormally Enhance Its Thermal Conductance. *Nano Letters* **2016**, *16*, 4954-4959.

67. Xu, X.; Pereira, L. F.; Wang, Y.; Wu, J.; Zhang, K.; Zhao, X.; Bae, S.; Bui, C. T.; Xie, R.; Thong, J. T. Length-Dependent Thermal Conductivity in Suspended Single-Layer Graphene. *Nature communications* **2014**, *5*, 3689.

68. Klemens, P.; Pedraza, D. Thermal Conductivity of Graphite in the Basal Plane. *Carbon* **1994**, *32*, 735-741.

69. Klemens, P. Theory of Thermal Conduction in Thin Ceramic Films. *International journal of thermophysics* **2001**, *22*, 265-275.

70. Hahn, K. R.; Melis, C.; Colombo, L. Thermal Transport in Nanocrystalline Graphene Investigated by Approach-to-Equilibrium Molecular Dynamics Simulations. *Carbon* **2016**, *96*, 429-438.

71. Sellan, D. P.; Landry, E. S.; Turney, J.; McGaughey, A. J.; Amon, C. H. Size Effects in Molecular Dynamics Thermal Conductivity Predictions. *Physical Review B* **2010**, *81*, 214305.

72. Hahn, K. R.; Melis, C.; Colombo, L. Effect of Structural Features on the Thermal Conductivity of Sige-Based Materials. *The European Physical Journal B* **2014**, *87*, 150.

73. Klemens, P. G. Theory of Thermal Conduction in Thin Ceramic Films. *International Journal of Thermophysics* **2001**, *22*, 265-275.

74. Li, Y.; Lin, Q.; Cui, D. Boundary-Dependent Mechanical Properties of Graphene Annular under in-Plane Circular Shearing Via Atomistic Simulations. *Scientific Reports* **2017**, *7*, 41767.

75. Tang, S.; Kulkarni, Y. The Interplay between Strain and Size Effects on the Thermal Conductance of Grain Boundaries in Graphene. *Applied Physics Letters* **2013**, *103*, 213113.

TOC Graphic

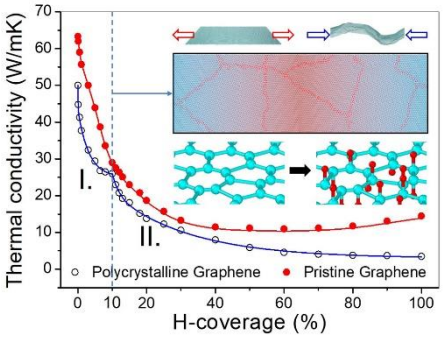
Thermal conductivity (W/mK)
70
60
50
40
30
20
10
0
I.
II.
Polycrystalline Graphene
Pristine Graphene
0
10
20
40
60
80
100
H-coverage (%)